Published in final edited form as:
Acta Biomater. 2009 May ; 5(4): 993–1005. doi:10.1016/j.actbio.2008.11.028.

Altered structural and mechanical properties in decellularized rabbit carotid arteries

C. Williams[a,*], **J. Liao**[b,c,†,*], **E.M. Joyce**[c], **B. Wang**[b], **J.B. Leach**[a,‡], **M.S. Sacks**[c], and **J.Y. Wong**[a,†]

a *Biomimetic Materials Engineering Laboratory, Department of Biomedical Engineering, Boston University, Boston, MA 02215, USA*

b *Cardiovascular Tissue Biomechanics Laboratory, Department of Agricultural and Biological Engineering, Mississippi State University, Mississippi State, MS 39762, USA*

c *Engineered Tissue Mechanics Laboratory, Department of Bioengineering, University of Pittsburgh, Pittsburgh, PA 15219, USA*

Abstract

Recently, major achievements in creating decellularized whole tissue scaffolds have drawn considerable attention to decellularization as a promising approach for tissue engineering. Decellularized tissues are expected to have mechanical strength and structure similar to the native tissues from which they are derived. However, numerous studies have shown that mechanical properties change after decellularization. Often, tissue structure is observed by histology and electron microscopy, but the structural alterations that may have occurred are not always evident. Here, a variety of techniques were used to investigate changes in tissue structure and relate them to altered mechanical behavior in decellularized rabbit carotid arteries. Histology and scanning electrom microscopy revealed that major extracellular matrix components were preserved and fibers appeared intact, although collagen appeared looser and less crimped after decellularization. Transmission electrom microscopy confirmed the presence of proteoglycans (PG), but there was decreased PG density and increased spacing between collagen fibrils. Mechanical testing and opening angle measurements showed that decellularized arteries had significantly increased stiffness, decreased extensibility and decreased residual stress compared with native arteries. Small-angle light scattering revealed that fibers had increased mobility and that structural integrity was compromised in decellularized arteries. Taken together, these studies revealed structural alterations that could be related to changes in mechanical properties. Further studies are warranted to determine the specific effects of different decellularization methods on the structure and performance of decellularized arteries used as vascular grafts.

Keywords

Decellularized artery; Extracellular matrix; Small-angle light scattering; Fiber orientation; Mechanical properties

†Corresponding authors: Tel.: +1 (662)3255987. E-mail address: E-mail: jliao@abe.msstate.edu (J. Liao); Tel: +1 (617)3532374. E-mail address: E-mail: jywong@bu.edu (J.Y. Wong).
*Co-first authors.
‡Present address: Department of Chemical and Biochemical Engineering, University of Maryland, Baltimore County, MD 21250, USA.

1. Introduction

Decellularized tissues have gained significant attention in the field of tissue engineering, especially for their promise in whole organ transplant and grafting [1,2]. Although most applications are still far from clinical use, numerous tissue types have been successfully decellularized, including heart [3], heart valve [4–7], bladder [1,8], blood vessel [9–11], skeletal muscle [12,13], tendon [14] and ligament [15,16]. A major motivation for using decellularized tissues is that they are expected to mimic closely the complex 3D structure and mechanical properties of the native tissues from which they are derived [17,18]. It is well established that the mechanical properties of a tissue are intimately linked to its structure [19], and this relationship is especially important for load-bearing tissues such as the artery [20].

Decellularized blood vessels have been studied extensively [9–11,21–34], mostly for their potential as scaffolds for small diameter vascular grafts (SDVG). There is a great need for tissue-engineered SDVG, as many patients do not have autologous vessels available and synthetic grafts are prone to failure in small diameter applications [35]; in many cases, this has been linked to inappropriate structure and/or mechanical performance [36,37]. If decellularized vessels do indeed maintain native tissue architecture and mechanical properties, these challenges could be overcome.

A majority of the literature regarding decellularized vessels tends to focus on cell seeding and implantation; while such studies are important and encouraging, there is still a lack of fundamental study of decellularized vessel structure–function relationships. Interestingly, many studies have reported that decellularized vessels have significantly altered mechanical characteristics compared with native vessels [10,11,21–23,29]. Histology and/or electron microscopy images are often included, but changes (or similarities) in extracellular matrix (ECM) structure are not necessarily evident. While these imaging techniques are commonly used and do provide some useful information on structure, they have limitations: specifically, they do not reveal whether fiber–fiber interactions, fiber orientation or fiber mobility changes as a result of decellularization, which are important to the structural integrity of tissue.

Preservation of ECM does not necessarily correspond to preservation of tissue architecture. Although the intention of most decellularization procedures is to minimize disruption to the ECM, the removal of cells inevitably results in changes to native ECM structure [17]. Therefore, the goal of the present study was to use a variety of characterization techniques to investigate tissue structure in decellularized rabbit carotid arteries and to relate structural changes to altered mechanical properties. Histology, transmission electron microscopy (TEM) and scanning electron microscopy (SEM) were used to confirm removal of cells and to assess qualitatively ECM composition and ultrastructure. Mechanical properties were determined using stress–strain analysis and stress relaxation tests; additionally, opening angle studies were used as a measure of residual stress in the vessel wall. Finally, small-angle light scattering (SALS), a quantitative technique that measures the average local fiber orientation throughout the tissue thickness [38], was used to determine gross fiber architecture and changes in ECM fiber kinematics (e.g., fiber mobility and organization). SALS was included to elucidate changes in structural integrity that would not be revealed from histology and EM alone. Together, these data provided insight into how altered structural properties could be related to changes in mechanical properties as a result of decellularization.

2. Materials and methods

2.1. Tissue harvest

All procedures were performed in accordance with the Institutional Animal Care and Use Committee at Boston University and the NIH Guide for the Care and Use of Laboratory Animals. Healthy male New Zealand white rabbits (2.5–3 kg, Pine Acres Rabbitry, Brattleboro, VT) were euthanized, and carotid arteries were harvested using sterile tools. Vessels were immediately placed in cold Hanks' Balanced Salt Solution (HBSS: 137 mM NaCl, 5.4 mM KCl, 0.42 mM Na_2HPO_4, 0.44 mM KH_2PO_4, 4.17 mM $NaHCO_3$, 10 mM HEPES, 5.55 mM glucose; 1% penicillin–streptomycin; pH 7.4) and stored on ice until use. For several samples, the length of the artery segment to be harvested was measured *in vivo* using digital calipers. The length was again measured after harvest, with the vessel in the unloaded state. The ratio of *in vivo* length to post-harvest length was determined (~1.7) and used for adjusting pressure-fixed samples to approximate *in vivo* length for the SALS studies described below.

2.2. Decellularization of carotid arteries

The decellularization procedure was modified from a previously published protocol [10]. First, carotid arteries were cleaned of blood and excess surrounding tissue. Vessels were then immersed in distilled water for 24 h at 4 °C to rupture cell membranes. Next, the vessels were treated with 0.025% trypsin (Gibco) diluted in Dulbecco's phosphate buffered saline (PBS; Gibco) for 24 h at 37 °C. After removal of trypsin, the vessels were treated with a solution of 1% TritonX-100 (Sigma) and 0.1% ammonium hydroxide (EM Science, Gibbstown, NJ) in distilled water for 72 h at 4 °C to remove nuclear components and lyse cell membranes and cytoplasmic proteins. Vessels were then transferred to a solution of Dulbecco's Modified Eagle Medium (DMEM; Gibco) with 5% bovine calf serum (BCS) to deactivate any residual trypsin for 24 h at 37 °C. Vessels were washed in distilled water for 24 h at 4 °C and, lastly, were washed overnight in PBS at 4 °C. All steps of the procedure were performed with mechanical agitation using a rotating platform.

2.3. Histology

For histological analysis, samples were fixed in 4% glutaraldehyde in PBS for 4 h, dehydrated with graduated concentrations of ethanol and embedded in paraffin. Cross-sections of the artery were cut to 5 μm thick. To elucidate changes in tissue components, Movat's Pentachrome stain was used to identify cells, collagen, elastin and PG with red, yellow, black and blue color, respectively. Stained tissue sections were imaged using bright field microscopy (Nikon EC600).

2.4. Transmission electron microscopy

Samples for TEM studies were fixed in 2% glutaraldehyde diluted in PBS overnight at 4 °C. For staining of PG, the specimens were fixed overnight in 1% Cupromeronic Blue (CB) under critical electrolyte concentration (CEC) conditions [39,40]. The 1% CB was in solution with 0.2 M acetate buffer (pH 5.6) containing 0.3 M $MgCl_2$. The specimen was then rinsed in a similar solution, excluding the CB stain. Following this rinse, the sample was immersed in 0.5% Na_2WO_4 in acetate buffer for 1 h, and overnight in 0.5% Na_2WO_4 in 30% ethanol. The specimens were rinsed in distilled water, stained with 1% uranyl acetate in 0.1 M acetate buffer for 1 h to reveal collagen fibrils. After being rinsed in 0.1 M maleate buffer and then in distilled water, the specimens were dehydrated with graduated concentration of ethanol and propylene oxide. Afterwards, the specimens were infiltrated and embedded in Epon, polymerized at 60 °C for 48 h. Ultra-thin sections (85 nm) were cut with a diamond knife and mounted on uncoated grids. Samples were then observed by TEM (JEOL JEM 100CXII).

2.5. Scanning electron microscopy

For SEM, a portion of the artery was cut open and two square sections were trimmed off in order to examine both the intimal and adventitial surfaces. Each section was fixed with 2.5% glutaraldehyde for 24 h, followed by three 15 min washes in PBS. Then, each section was subjected to sequential washes of 30, 50, 70, 90 and 100% ethanol. The specimens were left in each wash for 15 min and the 100% wash was performed three times. Next, specimens were subjected to critical point drying and gold sputter coating. Finally, SEM (JEOL 9335) was used to view the ultrastructure of the intimal and adventitial surfaces of the samples.

2.6. Mechanical testing

Uniaxial mechanical testing was carried out to assess the effect of decellularization on tissue mechanical properties using a Microforce Testing System (Tytron 250, Minneapolis, MN). The force and displacement resolutions of the device were 0.001 N and 0.0001 mm, respectively. Uniaxial tests were chosen as they have been frequently used to determine material properties of tissues and allow for straightforward calculation of the tangential modulus [10,20,21,32,41,42]. Native samples were stored frozen at −20 °C until use; frozen storage does not significantly affect artery mechanics [43]. Note that samples were not fixed in glutaraldehyde for mechanical tests. Experiments were carried out in a PBS bath at room temperature, as it has been shown that mechanical properties are not significantly different at room and body temperature [44]. Samples were tested in the axial direction and mounted on the testing device with two stainless steel grips cushioned with emery paper. The failure load for decellularized arteries was estimated in the pilot study. Approximately 10% of the failure load was then applied as the peak load for 10 cycles of preconditioning. All samples (decellularized n=4; native n=5) were then elongated to 0.6 N at a ramp speed of 0.1 mm s^{-1}. Tissue samples were kept slightly slack at the reference status. Gauge length, where the force increase initiated, was determined by analyzing the first derivatives of the force–displacement curve. Grip-to-grip strain normalized to gauge length was used to determine the Lagrangian strain for data analysis. Engineering stress was calculated by normalizing the force to initial cross-sectional area. Average artery diameter was estimated by imaging the specimens at load-free status, and wall thickness was estimated using a Mitutoyo gauge. Plotting the second derivative of the stress–strain curve revealed points corresponding to the onset of the linear region. Experimental data in the linear region were fit with linear regression. The tissue extensibility was defined as the intersecting point made by the extrapolation of the linear portion with the strain axis, and tensile modulus was the tangent of the linear fit. Hysteresis, a parameter that reflects energy dissipation, was measured by normalizing the enclosed area of the loading and unloading curves to the area underneath the loading curve. After stress–strain testing, each specimen was loaded to 0.6 N at a rate of 0.1 mm s^{-1} and held at this strain level for 1 h. Force decay over time was monitored, and the data were used to estimate the total amount of stress relaxation.

2.7. Opening angle measurements

Opening angles were used as a measurement of residual stress and strain in the arterial wall [45–49]. Experiments were performed at room temperature, as it has been shown that temperature in the range 20–37 °C does not significantly affect the opening angle [50]. Fresh native and decellularized samples (n=5 for each case) were cut into ring segments and equilibrated in physiological saline solution (119 mM NaCl, 4.7 mM KCl, 1.2 mM KH_2PO_4, 25 mM $NaHCO_3$, 1.2 mM $MgSO_4$, 2.5 mM $CaCl_2$, 10 mM glucose; pH=7.4) for 30 min. A single radial cut was made in each sample to relieve residual stresses, and the samples were again allowed to equilibrate for 30 min. Images of each sample in the zero stress state were then acquired at 5× magnification using an Axiovert-25 microscope (Carl Zeiss, Inc.) and Photron Fastcam Viewer software (version 2.4.3.8). When the sample did not fit in a single

image field, multiple images were taken with overlapping fields and later overlaid to form a single full image of each sample. The opening angle was defined as the angle formed between two lines extending from the tips of the opened sample to the midpoint of the inner arc of the sample and was measured using ImageJ 1.37.

2.8. Pressurized fixing of decellularized carotid arteries

For SALS studies, samples were prepared for both non-pressurized and pressurized conditions. For non-pressurized samples, the vessels were immersed in 4% glutaraldehyde (Polysciences, Inc., Warrington, PA) diluted in PBS overnight at 4 °C. For samples fixed at physiological length and pressure, a new protocol was developed due to the delicate and porous nature of decellularized arteries. After the first wash in distilled water, each end of the artery was cannulated onto a 1/16 in. female luer lock with tapered nozzle (Ark Plas Products, Flippin, AR) and carefully secured with epoxy. The vessel was kept moist while the epoxy set, and then the decellularization procedure resumed, continuing to completion. Native vessels were prepared the same day of harvest. For pressure fixing, the samples were connected to a tube system passing through a 100 mm Petri dish (Falcon) and stretched to approximate *in vivo* length. A CyQ 301 pressure display, CyQ 103 bridge–transducer interface, and Deltran blood pressure transducer (Utah Medical Products, Inc., Midvale, UT) were used to monitor pressure during the fixing procedure. A solution of 4% glutaraldehyde in glycerol (EM Science) was used to fix native and decellularized arteries under pressure. Glycerol was chosen because its high viscosity slowed down leakage from the decellularized arteries, which could not maintain pressure with PBS solution. Vessels were injected with the fixing solution, and pressure was increased to ~80 mmHg. The vessels were then covered with the fixing solution, and the pressure was monitored every 5 min for 2 h, and adjusted if necessary. Vessels were then rinsed well with PBS and stored in fresh PBS at 4 °C until use. Two decellularized and two native arteries were fixed in this manner.

2.9. Characterization of fiber architecture by SALS

SALS was used to reveal the fiber architecture in soft tissues [7,38,51,52]. Each sample was cut open longitudinally and dehydrated in graded solutions of glycerol/saline of 50, 75, 87 and 100% for 1 h each to clear the specimen, permitting an accurate light scattering measurement. Note that glycerol treatment did not cause distortion of the tissue's shape or structure [51,53]. The samples were then unfolded and SALS measurements were conducted over the entire tissue by raster scanning. A 5mW helium–neon continuous unpolarized wave laser (λ=632.8 nm) was passed through the tissue specimen, scattering light according to the internal planar fiber structure within the light beam envelope. The resulting angular distribution of scattered light intensity about the laser axis represented the distribution of fiber angles within the light beam envelope at the current tissue location. The preferred fiber direction was defined as the centroid of the fiber orientation distribution, so that equal areas (hence equal numbers of fibers) lay on either side of the centroid. The width of the intensity distribution was indicative of the degree of local fiber alignment: highly oriented fiber networks resulted in a very narrow peak, while more randomly distributed fibers yielded a broader peak. A physically intuitive orientation index (OI) was defined as the angle that contained half the total area under the intensity distribution, representing 50% of the total number of fibers. Thus, highly oriented fiber networks had low OI values, while more randomly oriented networks had larger values. The resulting data are presented as an overlaid vector map and color map, representing preferred fiber orientations and the degree of fiber alignment (i.e., OI), respectively, to show gross fiber architecture over the entire sample.

3. Results

3.1. Histology reveals the presence of PG and altered structure of adventitial collagen

Native carotid arteries showed characteristic arterial organization of cells and ECM with distinction between intimal, medial and adventitial layers (Fig. 1A); decellularized arteries also had distinct layers but contained no evidence of cells, and images showed that major ECM components were retained (Fig. 1B). At the magnifications shown, the endothelial cell layer that normally lines the native vessel lumen was not evident, but the internal elastic lamina was clearly observed in both native and decellularized arteries. The native media had alternating vascular smooth muscle cells (VSMC) and elastin-rich laminae (Fig. 1C). The elastic laminae of the decellularized artery appeared intact and morphologically similar to native vessels (Fig. 1D). Interestingly, the removal of cells revealed the presence of PG ground substance in the medial wall. The evidence of PG was surprising, as treatments with trypsin and TritonX-100 have been found to cause loss of PG [5,6,23,29]. Perhaps owing to the apparent preservation of PG, the thickness of the medial layer was not significantly reduced, as found with other decellularization methods [17,29]. Native adventitia contained many dense, wavy collagen fibers (Fig. 1C). Adventitial collagen was preserved in the decellularized artery, but appeared less compact and more extended compared with native (Fig. 1D), showing that loosening and uncrimping of the collagen fiber network occurred as a result of decellularization.

3.2. TEM confirms that PG are preserved after decellularization

To follow up on the histological evidence of PG, a TEM protocol that stains for PG and collagen fibrils was used (Fig. 2). TEM corroborated the presence of PG in both native and decellularized tissues, showing that the decellularization method used preserves PG, at least to some extent, in rabbit carotid arteries. Native samples had dense regions of collagen fibrils (Fig. 2A), but fibrils appeared less dense in decellularized tissue (Fig. 2B). In both native and decellularized arteries, PG decorated collagen fibrils at regular intervals (Fig. 2C, D). In the native artery, fibrils appeared to be closely associated in bundles, and PG appeared to interact with nearby fibrils. However, in the decellularized artery, spacing between fibrils seemed to be increased, along with a loss of PG density, suggesting decreased interaction between fibrils.

3.3. SEM shows fiber ultrastructure on intimal and adventitial surfaces

SEM further confirmed removal of cells and showed ECM ultrastructure on the intimal and adventitial surfaces of the vessels (Fig. 3). In the native artery, an intact layer of endothelial cells was present; note the corrugated surface due to wrinkling of the internal elastic lamina, and a small tear exposing basement membrane fibers underneath the cells (Fig. 3A). After decellularization, the cells were no longer present, and a network of fibers was revealed (Fig. 3B). Higher magnification showed detailed pore structures which appeared to be distinct holes that were previously occupied by cells; the fibers and pores suggested alignment, presumably in the same direction of endothelial cell alignment (Fig. 3C). Images of the adventitia confirmed histological observations: the native artery had a dense network of crimped, wavy collagen fibers (Fig. 3D), while the decellularized adventitia surface appeared almost smooth in places (Fig. 3E), with only shallow pores (Fig. 3F), suggesting significant uncrimping and extension of fibers. Of additional note, fibers appeared intact on both the intimal and adventitial surfaces of decellularized arteries, which may give the impression that the decellularization procedure did not damage the ECM; however, it is not evident from SEM whether fiber–fiber interactions were disrupted.

3.4. Changes in the mechanical properties and residual stresses of decellularized arteries

The mechanical properties of native and decellularized arteries were determined using uniaxial tests. Representative stress–strain curves are shown in Fig. 4A, and the mechanical

characteristics are summarized in Table 1. The tensile modulus for native arteries was significantly lower (2.29±0.24 MPa) than for decellularized arteries (3.48±0.72 MPa), showing that arteries became stiffer after decellularization. Additionally, native arteries had significantly greater extensibility (79.18±5.70%) compared with decellularized arteries (8.25 ±0.95%). However, hysteresis and stress relaxation (representative curves not shown) were not significantly different between native and decellularized arteries (31.55±12.60% vs 40.49 ±3.94% and 45.96±9.31% vs 52.91±6.35%, respectively). Mechanical testing showed that, although decellularized arteries demonstrated some viscoelastic behaviors similar to native tissue, there were also significant changes.

Native arteries had significantly greater opening angles compared with decellularized arteries (107±7.5° and 66.7±5.4°, respectively) (Fig. 4B–D), indicating that residual stress in the vessel wall decreased as a result of decellularization. Despite the apparent preservation of ECM components by histology, TEM and SEM, increased stiffness, decreased extensibility and decreased residual stress implies that significant fiber network disruptions had occurred.

3.5. Fiber kinematics of decellularized arteries

SALS was used to investigate fiber kinematics (changes in orientation and mobility) in decellularized vessels. At 0 mmHg, the native vessel fiber architecture map (Fig. 5A) showed that the preferred local fiber orientation (indicated by vectors) in many regions of the sample was toward the circumferential direction, and a prevalence of warm colors (low OI) indicated a high degree of alignment. The decellularized artery architecture map showed more random orientation of fibers and generally a lower degree of alignment (Fig. 5B). When samples were stretched to *in vivo* length and fixed at 80 mmHg, native vessel architecture maps showed swirling or S-shaped patterns of vectors (Fig. 6A, B), suggestive of a helical arrangement of fibers. Architecture maps of pressure-fixed decellularized arteries revealed that most fibers rotated towards the circumferential direction and became highly aligned (Fig. 6C, D).

Fig. 7 shows examples of fiber angular distribution plots for samples fixed at 0 and 80 mmHg. Note that fiber angular distribution plot examples are shown to illustrate differences in local alignment between decellularized and native arteries at 0 and 80 mmHg; global tissue organization can only be inferred from architecture maps in Figs. 4 and 5. At 0 mmHg, native artery distribution plots generally had narrow, symmetric peaks indicating high local alignment, while decellularized arteries typically had wide, multi-peaked distributions, indicating low local alignment and multiple preferred orientations (Fig. 7A). When pressurized to 80 mmHg, the shape of the fiber angular distribution for native arteries was similar to 0 mmHg, though slightly wider; however, the distribution for decellularized arteries became narrow and symmetric, indicating a high degree of local alignment (Fig. 7B). All together, SALS data showed that structural integrity was compromised in decellularized vessels, as highly mobile fibers were able to rotate easily towards the direction of applied strain. These structural changes are most likely attributed to high porosity and disruption to the ECM network as a result of decellularization.

4. Discussion

Decellularized vessels show potential as scaffolds for SDVG in clinical procedures, but often have altered mechanical properties compared with native arteries. Despite the importance of tissue structure to function, few studies have focused on decellularized vessel structure, even though removal of cells is certain to alter the native architecture of the ECM. This study sought to investigate and relate the changes in structural and mechanical properties of decellularized rabbit carotid arteries. Although the present study focuses on one type of vessel and a specific decellularization protocol, elucidating the altered structure–function relationship in decellularized tissues is of general interest. Determining what structural changes occur in

tissues will lead to greater understanding and predictability of their mechanical function [38]; furthermore, such knowledge would also be useful in predicting scaffold performance and in designing SDVG that more closely mimic the native artery.

4.1. Relating changes in mechanical properties to altered structure in decellularized arteries

Histology, TEM and SEM revealed several notable aspects of decellularized tissue structure, summarized as follows: (1) major ECM components were preserved, including PG; (2) elastic laminae of the media and fibers on the luminal and adventitial surfaces appeared intact; (3) there was a loosening and uncrimping of collagen fibers in the adventitia; and (4) spacing between collagen fibrils increased, with some loss of PG density. The first two points of interest, while initially encouraging from the perspective of SDVG design, did not allow the conclusion that no changes occurred in ECM interactions. The two latter observations showed that changes in structure had occurred and further implied that fiber interactions had been altered; however, the implications for gross tissue structural stability were not clear. SALS studies revealed an additional critical property of decellularized tissue structure: (5) fiber mobility was increased, allowing fibers to rotate easily towards the direction of applied strain. SALS data, therefore, were able to show that fiber–fiber interactions were changed or disrupted, leading to compromised structural integrity in decellularized arteries. In addition to these structural alterations, mechanical tests and opening angle studies demonstrated that decellularized vessels had increased stiffness, decreased extensibility and decreased residual stress compared with native arteries. The study now seeks to elucidate how changes in mechanical properties can be related to changes in structure for this particular study of decellularized rabbit carotid arteries.

Decellularized arteries became significantly stiffer than native arteries, which can be explained, at least in part, by the loosening and uncrimping of the collagen fiber network of the adventitia. In native arteries, a mixture of ECM components, particularly elastin and collagen, collectively contribute to mechanical behavior [20], resulting in a lower tensile modulus. It seems that the uncrimping of collagen in the decellularized artery leads to a more dominant collagen contribution to its mechanical behavior. Indeed, uncrimping of collagen fibers has been associated with increased stiffness in tissues [54]. Additionally, increased fiber mobility in decellularized arteries allowed fibers to reorient easily towards the direction of applied strain, which would lead to increased stiffness. Native arteries had greater structural integrity: higher numbers of fiber–fiber interactions and cell–fiber interactions could hinder fiber recruitment toward the direction of strain, resulting in a less stiff tissue.

Decellularized arteries experienced a significant decrease in extensibility compared with native arteries. The combination of highly extensible elastin and waviness of collagen fibers is responsible for high extensibility in native arteries [20,54]. In stress–strain curves (Fig. 4A), this is evident in the long toe region, which corresponds to increasing fiber recruitment as crimped collagen fibers extend and align in the direction of strain [54]. The short toe region in the stress–strain curve of decellularized vessels is related to the observation that fibers were already substantially uncrimped, and thus were rapidly recruited to the direction of applied strain at low values.

A decreased opening angle in decellularized arteries demonstrated that residual stresses were relieved, and is consistent with other findings in decellularized arteries [29]. It is unlikely that uncrimping of collagen significantly contributed to decreased opening angle, as residual stresses are generally attributed to elastin [55] and VSMC which can actively modulate stress in the vessel wall [56]. As elastic laminae in decellularized arteries appeared intact and wavy, similar to native arteries, the decreased opening angle is most likely due to removal of cells, resulting in increased porosity and disruption of cell–fiber interactions that allowed residual stresses to be released. This is also supported by SALS, which demonstrated a loss of structural

stability after decellularization. Additionally, there is evidence for PG function in residual stress in the vessel wall [57]; thus, loss of PG density could have contributed to decreased opening angles in decellularized arteries.

It is possible that structural changes not apparent from these studies occurred which affected the mechanical behavior in decellularized arteries. For example, the combination of decellularization reagents and 1-week processing time could have led to damage or calcification of elastin [17,34], which would have contributed to increased stiffness, decreased extensibility and decreased opening angle [46,55,58,59]. Note, however, that these possible changes are only speculative and are offered for the sake of thorough discussion, as histology did not reveal any morphological differences between the elastic laminae of native and decellularized arteries.

Finally, the similarities found in viscoelastic characteristics of native and decellularized arteries were surprising and worth discussing. Hysteresis was not significantly affected by decellularization. This result was interesting because increased fiber mobility in decellularized arteries might be expected to correlate with increased hysteresis. The lack of difference in hysteresis might be the result of decreased ECM interactions after decellularization. Although decellularized arteries had higher fiber mobility than native tissue, they also had looser collagen fiber networks and loss of PG density, leading to greater freedom of movement with less contact between fibers. However, native arteries had a dense, crimped collagen network and high density of PG which most likely resulted in more points of frictional contact. Additionally, native arteries contained VSMC, which are highly viscoelastic and known to contribute significantly to hysteresis [60]. Decellularized vessels also showed similar stress relaxation behavior compared with native arteries, despite the loss of VSMC, which are thought to play a major role in the stress relaxation phenomenon [20]. However, VSMC modulation of stress relaxation depends on contractile activity [61]; therefore, in the absence of VSMC stimulation, the stress relaxation response in both native and decellularized arteries was probably due to passive reorganization of ECM.

4.2. Compromised structural integrity in decellularized arteries

Altered fiber kinematics merits further attention, as SALS data revealed that the structural stability of decellularized vessels was compromised (Figs. 5–7). At 0 mmHg, native arteries showed a high degree of fiber alignment in the circumferential direction (Fig. 5A). As the vessel contracted to nearly half its original length upon harvest, it is not surprising that most of the fibers throughout the wall thickness would assume circumferential orientation, including adventitial fibers, which tend to have a more disorganized or longitudinal orientation *in vivo* [62,63]. However, decellularized vessels demonstrated a lower degree of alignment and more random orientation of fibers, despite being in a similar unloaded state (Fig. 5B). However, this is consistent with the argument that looser fibers with a disrupted network would be more disorganized in the absence of physiological pressure and tension. This finding alone indicated a loss of structural integrity resulting from increased porosity and loss of cell–fiber and fiber–fiber interactions during the decellularization process.

Increased fiber mobility in decellularized arteries was demonstrated when samples were fixed at physiological length and pressure. In native arteries, swirling or S-shaped patterns in architecture maps suggested a helical organization of fibers (Fig. 6A, B). Helical structure has been found in pig carotid artery, and evidence suggests that it exists to varying degrees in other vessels and species [62]. However, it is also possible that the helical pattern represented two populations of fiber orientation: the circumferential organization typically seen in the media and the longitudinal organization often characteristic of the adventitia [63]. Nonetheless, the change from circumferential to helical organization in native arteries represents a stable structure, similar to a coiled spring that can expand and retract. However, this structural stability

was compromised in decellularized arteries, as most fibers throughout the vessel wall became oriented toward the circumferential direction and were highly aligned (Fig. 6C, D). The high mobility of fibers in decellularized arteries further showed that ECM network associations were disrupted. Increased fiber mobility would allow for significant reorientation of fibers at low strains, and is consistent with mechanical data (e.g., the short toe region of the stress–strain). This is less true for the native artery, which has been shown to have stable structure over a range of physiological pressures [64]. Thus, the change from randomly oriented to highly aligned fibers in decellularized arteries indicates that the structure is unstable and highly dependent on applied strains.

Although SALS did not reveal what specific fiber network interactions were altered or destroyed, TEM points to changes in collagen fibril interactions mediated by PG. Decreased PG density and increased spacing between collagen fibrils implies that interaction between fibrils would be less in decellularized arteries compared with native ones. PG are known to serve as cross-linking agents in collagen micro-fibril assembly, associating with collagen primarily at D period banding sites [54]. Studies suggest that PG help transfer load between collagen fibrils [40,65] and/or provide stability to fiber networks [66]. Therefore, decreased PG-mediated interaction between collagen fibrils most likely contributes to increased fiber mobility and loss of structural stability in decellularized arteries.

4.3. Limitations of study

Although it is hoped that the present study may shed light on improving SDVG design, the goal was not to develop a scaffold suitable for implantation as a vascular graft. Rather, the aim was to elucidate how the structure–function relationship is altered in decellularized arteries. Therefore, studies of endothelial cell adhesion or anti-thrombogenetic properties of decellularized vessels were not included. Further, no biomechanical tests were performed that required inflation of the intact vessel (e.g., pressure–diameter, burst pressure). Although such tests are important for engineered vascular grafts, they could not be done with the decellularized arteries. This was because the vessels became highly porous after decellularization and could not hold steady pressure, as noted during pressurized fixing. Uniaxial tests were therefore used to determine material properties of interest.

Rabbit carotid arteries and a specific decellularization protocol were used as the model system. This is a limitation, because it would be valuable to investigate several decellularization methods and determine which is “ideal” for a vascular graft. Several studies have already compared the effects of different decellularization techniques on tissues [7,23], although surely there is more work to be done in this area. Nevertheless, as the changes that occur during decellularization are highly dependent on species, vessel (or other tissue) type and method [17], it would be difficult to compare the present results with other studies, regardless of whether one method was investigated or several. Instead, the authors were interested in studying one model system in depth to highlight what changes can occur in structure and mechanical properties as a result of decellularization. It is hoped that these results, though specific, will motivate further studies of other tissues and decellularization protocols in general.

Although SALS is a powerful technique for investigating gross tissue architecture, it has several limitations. Of primary concern was the need to cut samples open, as the SALS system requires planar samples. While this action changes the geometry of the vessels, fiber organization should remain unaffected as a result of fixing the samples in glutaraldehyde. While the effects of glutaraldehyde fixation are complex and not fully understood, it has been shown to preserve ultrastructure well. The results for native samples appeared consistent with what is known about native artery structure, and the findings for decellularized samples agreed with what was learned from histology, TEM, SEM and mechanical studies. Therefore, it is felt that sample preparation for SALS did not confound the results. Additionally, SALS reveals average fiber

structure throughout the whole tissue thickness; therefore, contributions from individual layers could not be determined. Finally, SALS could not reveal the degree to which changes in porosity, cell–ECM interactions and fiber–fiber interactions specifically contributed to altered structural and mechanical properties in decellularized arteries. Determining the individual contributions of these factors to altered structure–function relationships is therefore of interest for future work.

5. Conclusion

It was found that decellularized arteries had a looser, uncrimped collagen network, which could explain increased stiffness and decreased extensibility compared with native arteries. Additionally, increased fiber mobility in decellularized arteries was related to increased stiffness, as fibers could easily rotate toward the direction of strain. High fiber mobility also led to disrupted structural stability due to increased porosity from removal of cells, as well as altered collagen interaction suggested by increased fibril spacing and decreased PG density. Altered structural and mechanical properties as a result of decellularization have important implications for vascular tissue engineering. Compliance mismatch is a common mode of failure in vascular grafts [67] and cell behavior, including adhesion, migration and proliferation, is affected by altered matrix, fiber organization and tissue stiffness [68–70]. The present study has focused on one decellularization method and one type of blood vessel; the authors acknowledge that the effects of decellularization on structure–function relationships will change significantly, depending on method and even vessel type. Future studies are warranted to elucidate the specific effects of altered structure–function relationships on the overall fate of decellularized vessels used in vascular tissue engineering applications.

Acknowledgements

This work was supported by NIH (HL72900) to JYW, AHA pre-doctoral fellowship to CW, and AHA BGIA (0565346U) to JL. MSS is an Established Investigator of the AHA. The authors would like to thank Jennifer Debarr, Mark Rubin and Amanda Lawrence for histology, SEM and TEM observations. The authors are also grateful to Erzsebet Bartolak-Suki for insightful discussions and critical review of the manuscript.

References

1. Atala A, Bauer SB, Soker S, Yoo JJ, Retik AB. Tissue-engineered autologous bladders for patients needing cystoplasty. The Lancet 2006;367:1241.
2. Wang X, Lin P, Yao Q, Chen C. Development of small-diameter vascular grafts. World J Surg 2007;31:682. [PubMed: 17345123]
3. Ott HC, Matthiesen TS, Goh S-K, Black LD, Kren SM, Netoff TI, Taylor DA. Perfusion-decellularized matrix: using nature's platform to engineer a bioartificial heart. Nature Medicine 2008;14:213.
4. Bader A, Schilling T, Teebken OE, Brandes G, Herden T, Steinhoff G, Haverich A. Tissue engineering of heart valves - human endothelial cell seeding of detergent acellularized porcine valves. Eur J Cardio-thoracic Surg 1998;14:279.
5. Grauss RW, Hazekamp MG, Oppenhuizen F, Munsteren CJv, Groot ACG-d, DeRuiter MC. Histological evaluation of decellularised porcine aortic valves: matrix changes due to different decellularisation methods. Eur J Cardio-thoracic Surg 2005;27:566.
6. Schenke-Layland K, Vasilevski O, Opitz F, Konig K, Riemann I, Halbhuber KJ, Wahlers T, Stock UA. Impact of decellularization of xenogenic tissue on extracellular matrix integrity for tissue engineering of heart valves. J Struct Biol 2003;143:201. [PubMed: 14572475]
7. Liao J, Joyce EM, Sacks MS. Effects of decellularization on the mechanical and structural properties of the porcine aortic valve leaflet. Biomaterials 2008;29:1065. [PubMed: 18096223]
8. Chen F, Yoo JJ, Atala A. Acellular collagen matrix as a possible "off the shelf" biomaterial for urethral repair. Urology 1999;54:407. [PubMed: 10475343]

9. Conklin BS, Richter ER, Kreutziger KL, Zhong DS, Chen C. Development and evaluation of a novel decellularized vascular xenograft. Med Eng Phys 2002;24:173. [PubMed: 12062176]
10. Amiel GE, Komura M, Shapira O, Yoo JJ, Yazdani S, Berry J, Kaushal S, Bischoff J, Atala A, Soker S. Engineering of blood vessels from acellular collagen matrices coated with human endothelial cells. Tissue Eng 2006;12:2355. [PubMed: 16968175]
11. McFetridge PS, Daniel JW, Bodamyali T, Horrocks M, Chaudhuri JB. Preparation of porcine carotid arteries for vascular tissue engineering applications. J Biomed Mater Res 2004;70A:224.
12. Moon DG, Christ G, Stitzel JD, Atala A, Yoo JJ. Cyclic mechanical preconditioning improves engineered muscle contraction. Tissue Eng 2008;14:473.
13. Borschel GH, Dennis RG Jr. WMK Contractile skeletal muscle tissue-engineered on an acellular scaffold. Plast Reconstr Surg 2004;113:595. [PubMed: 14758222]
14. Cartmell JS, Dunn MG. Effect of chemical treatments on tendon cellularity and mechanical properties. J Biomed Mater Res 2000;49:134. [PubMed: 10559756]
15. Ingram JH, Korossis S, Howling G, Fisher J, Ingham E. The use of ultrasonication to aid recellularization of acellular natural tissue scaffolds for use in anterior cruciate ligament reconstruction. Tissue Eng 2007;13:1561. [PubMed: 17518726]
16. Tischer T, Vogt S, Aryee S, Steinhauser E, Adamczyk C, Milz S, Martinek V, Imhoff AB. Tissue engineering of the anterior cruciate ligament: a new method using acellularized tendon allografts and autologous fibroblasts. Arch Orthop Trauma Surg 2007;127:735. [PubMed: 17541614]
17. Gilbert TW, Sellaro TL, Badylak SF. Decellularization of tissues and organs. Biomaterials 2006;27:3675. [PubMed: 16519932]
18. Stegemann JP, Kaszuba SN, Row SL. Advances in vascular tissue engineering using protein-based biomaterials. Tissue Eng 2007;13ahead of print
19. Fung, YC. Biomechanics: Mechanical Properties of Living Tissues. New York: Springer; 1993.
20. Dobrin PB. Mechanical properties of arteries. Physiol Rev 1978;58:397. [PubMed: 347471]
21. Chang Y, Hsu CK, Wei HJ, Chen SC, Liang HC, Lai PH, Sung HW. Cell-free xenogenic vascular grafts fixed with glutaraldehyde or genipin: in vitro and in vivo studies. J Biotechnol 2005;120:207. [PubMed: 16112218]
22. Borschel GH, Huang Y-C, Calve S, Arruda EM, Lynch JB, Dow DE, Kuzon WM, Dennis RG, Brown DL. Tissue engineering of recellularized small-diameter vascular grafts. Tissue Eng 2005;11:778. [PubMed: 15998218]
23. Dahl SLM, Koh J, Prabhakar V, Niklason LE. Decellularized native and engineered arterial scaffolds for transplantation. Cell Transplant 2003;12:659. [PubMed: 14579934]
24. Goissis G, Suzigan S, Parreira DR, Maniglia JV, Braile DM, Raymundo S. Preparation and characterization of collagen-elastin matrices from blood vessels intended as small diameter vascular grafts. Artif Organs 2000;24:217. [PubMed: 10759645]
25. Hilbert SL, Boerboom LE, Livesey SA, Ferrans VJ. Explant pathology study of decellularized carotid artery vascular grafts. J Biomed Mater Res 2004;69A:197.
26. Huynh T, Abraham G, Murray J, Brockbank K, Hagen P-O, Sullivan S. Remodeling of an acellular collagen graft into a physiologically responsive neovessel. Nature Biotechnol 1999;17:1083. [PubMed: 10545913]
27. Jo WM, Sohn YS, Choi YH, Kim HJ, Cho HD. Modified acellularization for successful vascular xenotransplantation. J Korean Med Sci 2007;22:262. [PubMed: 17449935]
28. Lu Q, Ganesan K, Simionescu DT, Vyavahare NR. Novel porous aortic elastin and collagen scaffolds for tissue engineering. Biomaterials 2004;25:5227. [PubMed: 15110474]
29. Roy S, Silacci P, Stergiopulos N. Biomechanical properties of decellularized porcine common carotid arteries. Am J Physiol Heart Circ Physiol 2005;289:H1567. [PubMed: 15908462]
30. Schaner PJ, Martin ND, Tulenko TN, Shapiro IM, Tarola NA, Leichter RF, Carabasi RA, DiMuzio PJ. Decellularized vein as a potential scaffold for vascular tissue engineering. J Vasc Surg 2004;40:146. [PubMed: 15218475]
31. Antonova ML, Antonov PS, Marinov GR, Vlaskovska MV, Kasakov LN. Viscoelastic characteristics of in vitro vital and devitalized rat aorta and human arterial prostheses. Ann Biomed Eng 2008;36:947. [PubMed: 18330704]

32. Huang HM, Wu SF, Hong R. Tissue-engineered graft constructed by self-dereived cells and heterogeneous acellular matrix. J Zhe Univ Sci B 2006;7:351.
33. Ketchedjian A, Jones AL, Krueger P, Robinson E, Crouch K, Wolfinbarger L, Hopkins R. Recellularization of decellularized allograft scaffolds in ovine great vessel reconstructions. Ann Thorac Surg 2005;126:888. [PubMed: 15734400]
34. Price PA, Chan WS, Jolson DM, Williamson MK. The elastic lamellae of devitalized arteries calcify when incubated in serum: evidence for a serum calcification factor. Arterioscler Thromb Vasc Biol 2006;26:1079. [PubMed: 16528009]
35. L'Heureux N, Dusserre N, Marini A, Garrido S, Fuente Ldl, McAllister T. Technology Insight: the evolution of tissue-engineered vascular grafts—from research to clinical practice. Nature Clinical Practice Cardiovasc Med 2007;4:389.
36. Canham PB, Finlay HM, Boughner DR. Contrasting structure of the saphenous vein and internal mammary artery used as coronary bypass vessels. Cardiovasc Res 1997;34:557. [PubMed: 9231039]
37. Couet F, Rajan N, Mantovani D. Macromolecular biomaterials for scaffold-based vascular tissue engineering. Macromolec Biosci 2007;7:701.
38. Sacks MS, Smith DB, Hiester ED. A small angle light scattering device for planar connective tissue microstructural analysis. Ann Biomed Eng 1997;25:678. [PubMed: 9236980]
39. Haigh M, Scott JE. A method of processing tissue sections for staining with cu-promeronic blue and other dyes, using CEC techniques, for light and electron microscopy. Basic Appl Histochem 1986;30:479. [PubMed: 2435276]
40. Liao J, Vesely I. Skewness angle of interfibrillar proteoglycans increases with applied load on chordae tendinae. J Biomech 2007;40:390. [PubMed: 16483580]
41. Black LD, Brewer KK, Morris SM, Schreiber BM, Toselli P, Nugent MA, Suki B, Stone PJ. Effects of elastase on the mechanical and failure properties of engineered elastin-rich matrices. J Appl Physiol 2005;98:1434. [PubMed: 15640390]
42. Wang P, Shu Z, He L, Chen S, Wang Y, Wang XL. The structural and cellular viability in cryopreserved rabbit carotid arteries. J Surg Res 2006;131:241. [PubMed: 16427085]
43. Stemper BD, Yoganandan N, Stineman MR, Gennarelli TA, Baisden JL, Pintar FA. Mechanics of fresh, refrigerated, and frozen arterial tissue. J Surg Res 2007;139:236. [PubMed: 17303171]
44. Schaar JA, Korte CLd, Mastik F, Steen AFWvd. Effect of temperature increase and freezing on intravascular elastography. Ultrasonics 2002;40:879. [PubMed: 12160062]
45. Chuong CJ, Fung YC. On residual stresses in arteries. J Biomech Eng 1986;108:189. [PubMed: 3079517]
46. Matsumoto T, Hayashi K, Ide K. Residual strain and local strain distributions in the rabbit atherosclerotic aorta. J Biomech 1995;28:1207. [PubMed: 8550639]
47. Zhao J, Day J, Yuan ZF, Gregersen H. Regional arterial stress–strain distributions referenced to the zero-stress state in the rat. Am J Physiol Heart Circ Physiol 2002;282:H622. [PubMed: 11788411]
48. Rachev A, Hayashi K. Theoretical study of the effects of vascular smooth muscle contraction on strain and stress distributions in arteries. Ann Biomed Eng 1999;27:459. [PubMed: 10468230]
49. Rachev A, Greenwald SE. Residual strains in conduit arteries. J Biomech 2003;36:661. [PubMed: 12694996]
50. Frobert O, Gregersen H, Bjerre J, Bagger JP, Kassab GS. Relation between zero-stress state and branching order of porcine left coronary arterial tree. Am J Physiol Heart Circ Physiol 1998;275:2283.
51. Sacks MS, Smith DB, Hiester ED. The aortic valve microstructure: effects of transvalvular pressure. J Biomed Mater Res 1998;41:131. [PubMed: 9641633]
52. Sacks MS, Schoen FJ. Collagen fiber disruption occurs independent of calcification in clinically explanted bioprosthetic heart valves. J Biomed Mater Res 2002;62:359. [PubMed: 12209921]
53. Fahner PJ, Idu MM, Legemate DA, Vanbavel E, Borstlap J, Pfaffendorf M, Marle Jv, Gulik TMv. Morphological and functional alterations in glycerol preserved rat aortic allografts. Int J Artif Organs 2004;27:979. [PubMed: 15636056]
54. Freed AD, Doehring TC. Elastic model for crimped collagen fibrils. J Biomech Eng 2005;127:587. [PubMed: 16121528]

55. Greenwald SEJE, Moore J, Rachev A, Kane TPC, Meister JJ. Experimental investigation of the distribution of residual strains in the artery wall. J Biomech Eng 1997;119:438. [PubMed: 9407283]
56. Matsumoto T, Tsuchida M, Sato M. Change in intramural strain distribution in rat aorta due to smooth muscle contraction and relaxation. Am J Physiol 1996;271:H1711. [PubMed: 8897968]
57. Azeloglu EU, Albro MB, Thimmappa VA, Ateshian GA, Costa KD. Heterogeneous transmural proteoglycan distribution provides a mechanism for regulating residual stresses in the aorta. Am J Physiol Heart Circ Physiol 2008;294:H1197. [PubMed: 18156194]
58. Atkinson J. Age-related medial elastocalcinosis in arteries: mechanisms, animal models and physiological consequences. J Appl Physiol. 2008in press
59. Lee TC, Midura RJ, Hascall VC, Vesely I. The effect of elastin damage on the mechanics of the aortic valve. J Biomech 2001;34:203. [PubMed: 11165284]
60. Holzapfel, GA.; Ogden, RW., editors. Biomechanics of Soft Tissue in Cardiovascular Systems. New York: Springer-Verlag; 2003.
61. Seidel CL, Murphy RA. Stress relaxation in hog carotid artery as related to contractile activity. Blood Vessels 1976;13:78. [PubMed: 1247696]
62. Rhodin, JAG. Handbook of Physiology—The Cardiovascular System II. 1979. Architecture of the vessel wall; p. 1
63. Krause, WJ. The Art of Examining and Interpreting Histologic Preparations: A Laboratory Manual and Study Guide for Histology. Boca Raton, FL: Universal Publishers; 2004.
64. Finlay HM, Dixon JG, Canham PB. Fabric organization of the subendothelium of the human brain artery by polarized-light microscopy. Arterioscler Thromb Vasc Biol 1991;11:681.
65. Liao J, Yang L, Grashow J, Sacks MS. The relation between collagen fibril kinematics and mechanical properties in the mitral valve anterior leaflet. J Biomech Eng 2007;129:78. [PubMed: 17227101]
66. Cavalcante FSA, Ito S, Brewer K, Sakai H, Alencar AM, Almeida MPJS, Andrade J, Majumdar A, Ingenito EP, Suki B. Mechanical interactions between collagen and proteoglycans: implications for the stability of lung tissue. J Appl Physiol 2005;98:672. [PubMed: 15448123]
67. Kapadia MR, Popowich DA, Kibbe MR. Modified prosthetic vascular conduits. Circulation 2008;117:1873. [PubMed: 18391121]
68. Gratzer PF, Harrison RD, Woods T. Matrix alteration and not residual sodium dodecyl sulfate cytotoxicity affects the cellular repopulation of a decellularized matrix. Tissue Eng 2006;12:2975. [PubMed: 17518665]
69. Curtis A, Wilkinson C. Topographical control of cells. Biomaterials 1997;18:1573. [PubMed: 9613804]
70. Brown XQ, Ookawa K, Wong JY. Evaluation of polydimethylsiloxane scaffolds with physiologically-relevant elastic moduli: interplay of substrate mechanics and surface chemistry effects on vascular smooth muscle cell response. Biomaterials 2005;26:3123. [PubMed: 15603807]

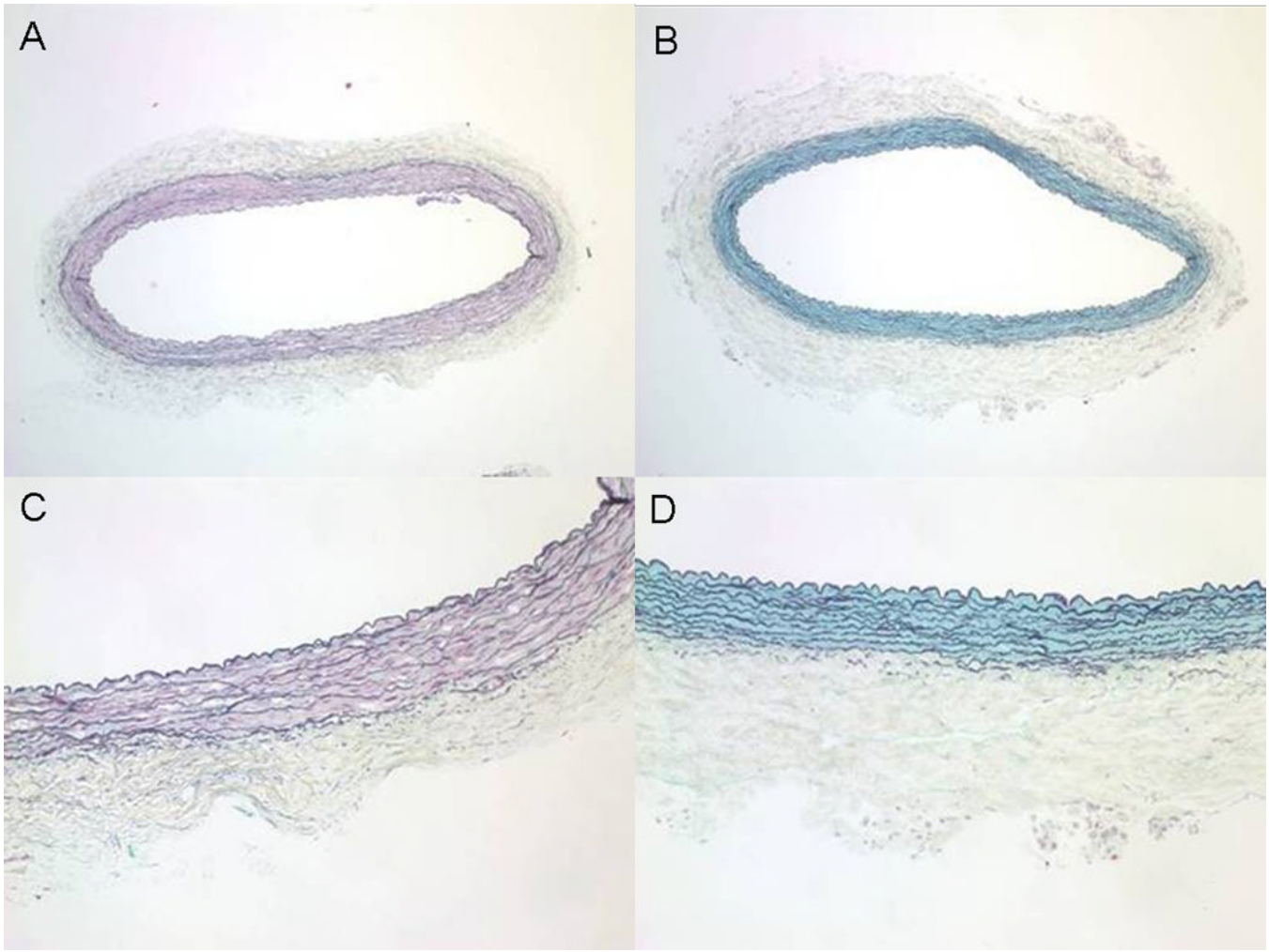

Fig. 1.

Histology of native and decellularized carotid arteries. Whole cross-section of (A) native and (B) decellularized arteries with Movat's pentachrome stain showing cells (red/pink), elastin (black), collagen (yellow) and proteoglycans (blue). Higher magnification images of (C) native and (D) decellularized samples show in greater detail that the decellularization procedure removed cells from the vessel wall while preserving major ECM components; however, there appears to be loosening and uncrimping of collagen in the adventitia after decellularization. A and C: 4× magnification; B and D: 10× magnification.

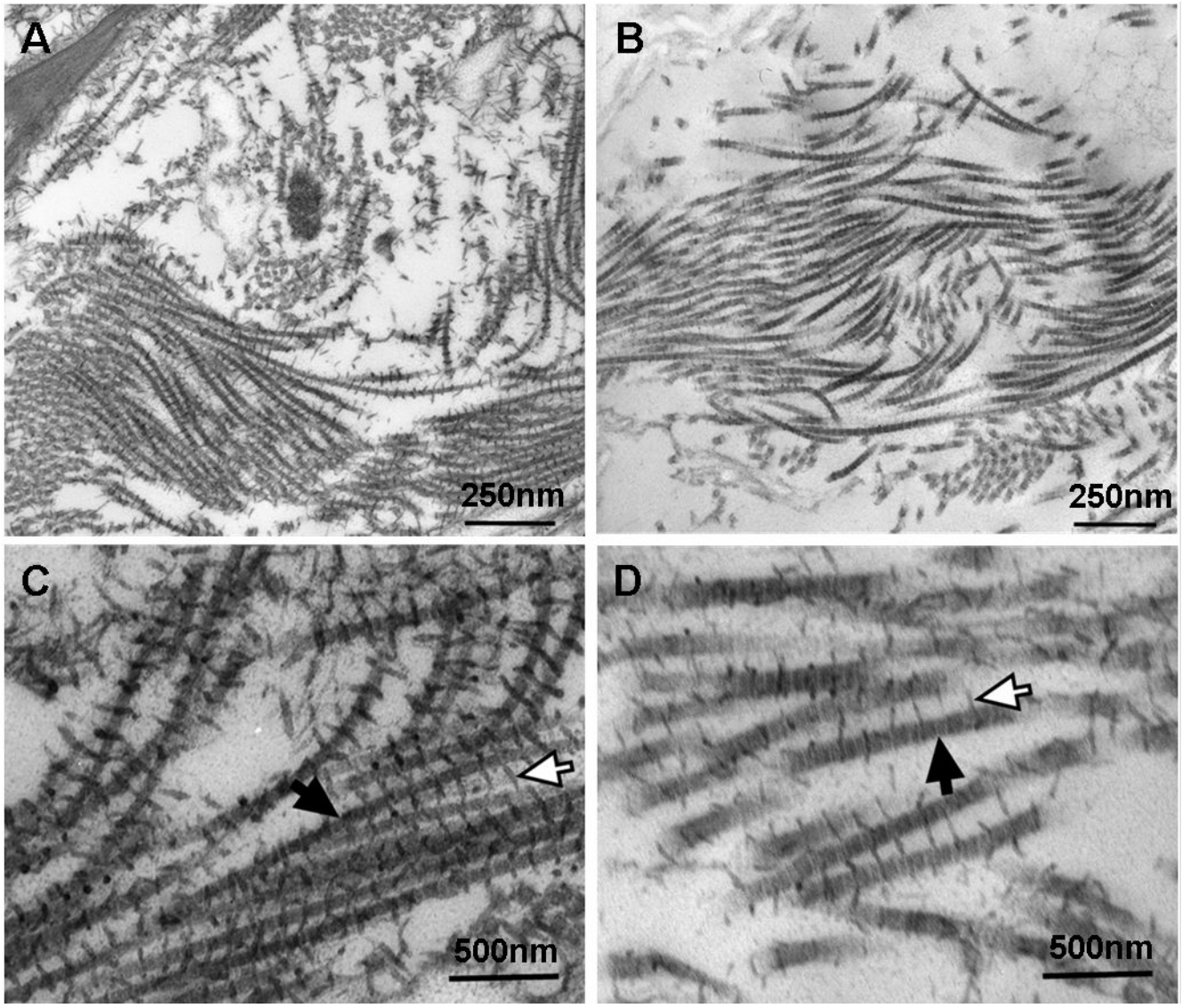

Fig. 2.

TEM of decellularized and native arteries. Example images are shown for (A) native and (B) decellularized arteries stained for PG. Native tissue appears denser than decellularized. Zoomed-in images of (C) native and (D) decellularized samples show details of PG (open arrows) decorating collagen fibrils (solid arrows). Although decellularization preserved PG, there appears to be some loss in density.

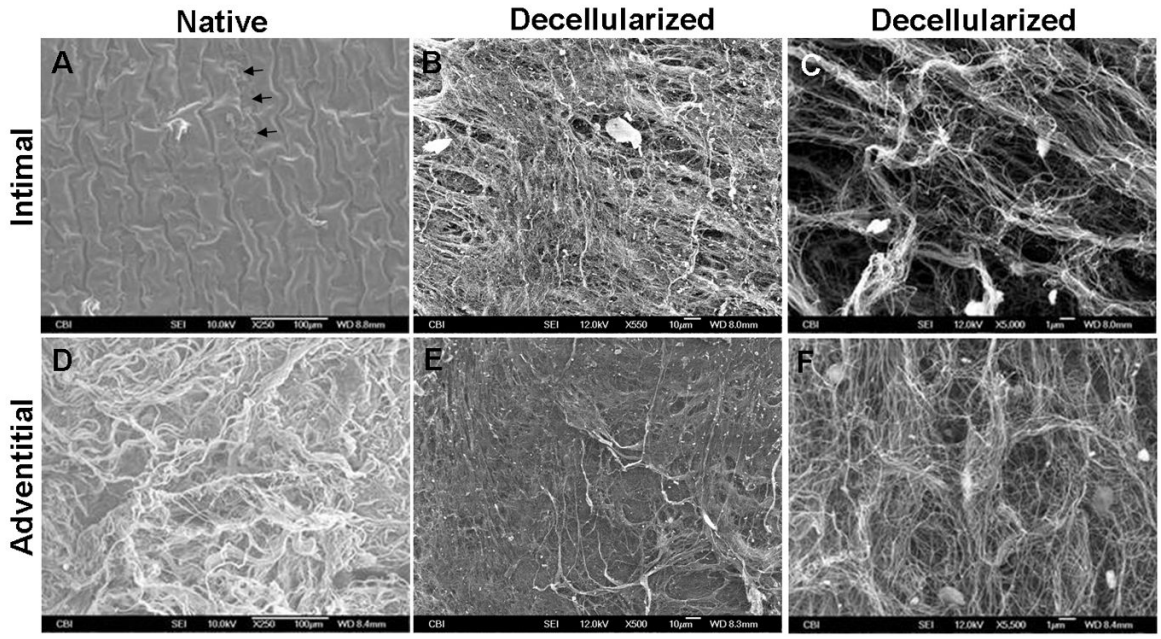

Fig. 3.

SEM of intimal and adventitial surfaces of native and decellularized arteries. (A) The intima of the native vessel shows a corrugated endothelial layer; a small tear shows exposed basement membrane underneath (arrows). (B) The intima of the decellularized artery shows exposed ECM. (C) Higher magnification reveals detailed pore structure. (D) The adventitial surface of the native artery has thick bundles of crimped collagen fibers. (E) The adventitia of the decellularized artery has a smoother surface, suggesting uncrimping of fibers. (F) Higher magnification of the decellularized adventitial surface shows detail of shallow pores and fibers.

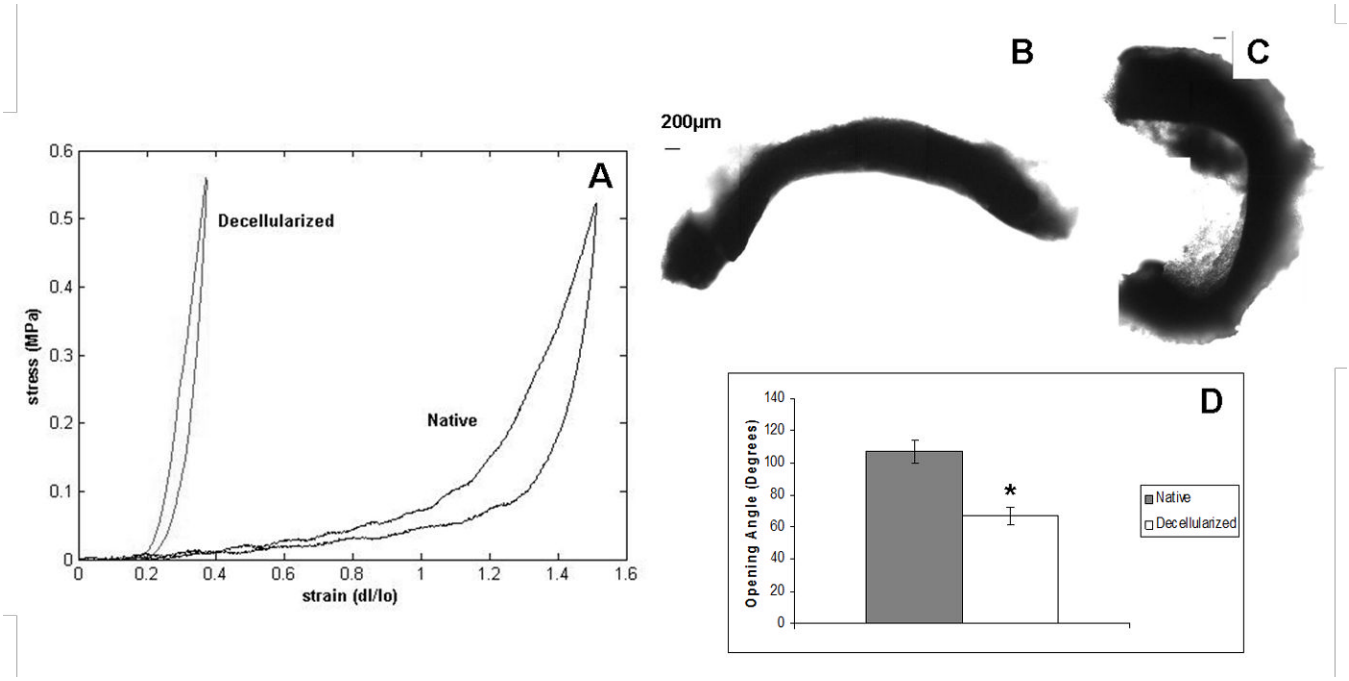

Fig. 4.

Mechanical properties and opening angles for native and decellularized carotid arteries. (A) Representative stress–strain curves for native (black) and decellularized (gray) arteries. Decellularized arteries were significantly stiffer and less extensible than native arteries. Mechanical properties are summarized in Table 1. Representative images for (B) native and (C) decellularized arteries cut for opening angle measurements. (D) Opening angles were significantly greater in native arteries compared with decellularized ones, indicating a significant decrease in residual stresses after decellularization. * Indicates significantly different from native for $P<0.05$.

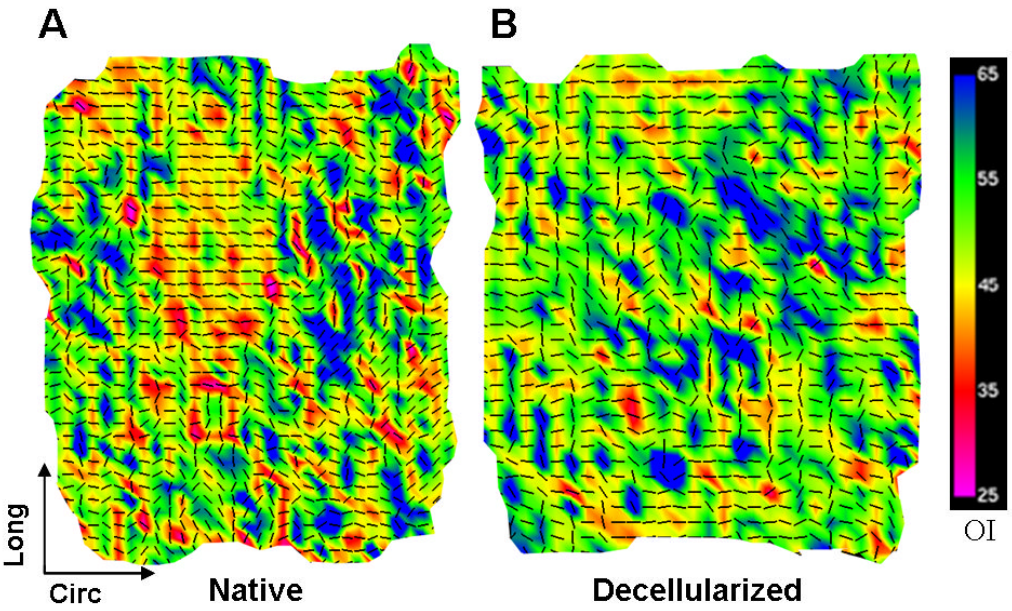

Fig. 5.

Fiber kinematics for non-pressurized arteries. Fiber architecture maps for (A) native and (B) decellularized arteries fixed at 0 mmHg. Black vectors represent the preferred local fiber orientations, and colors represent OI; warmer colors represent lower OI, which indicates a higher degree of alignment. Native arteries showed a high degree of fiber alignment towards the circumferential direction. Decellularized arteries had more random fiber orientation and lower alignment (higher prevalence of cooler OI colors), suggesting structural interruption.

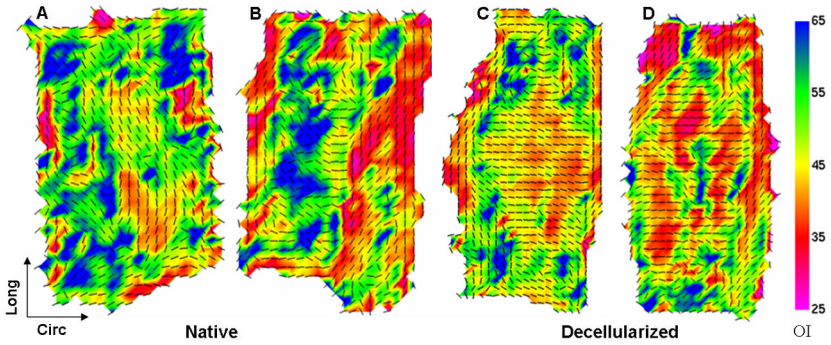

Fig. 6.

Fiber kinematics for pressure-fixed arteries. (A, B) Native and (C, D) decellularized arteries were stretched to approximate *in vivo* length and fixed at a pressure of 80 mmHg. Native vessel architecture maps indicate a helical, evidenced by the swirling pattern of vectors. In decellularized arteries, the fiber orientation maps show that most fibers throughout the vessel wall rotated towards the circumferential direction and became highly aligned, indicating high fiber mobility.

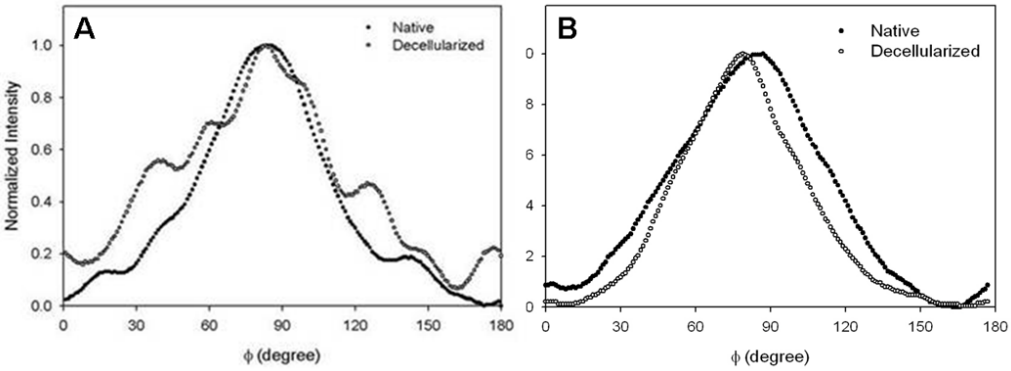

Fig. 7.

Changes in fiber organization in native and decellularized vessels. Example fiber angular distribution plots are shown for native (solid circles) and decellularized (open circles) arteries at 0 mmHg (A) and 80 mmHg (B). Note that the distribution plots are shown to illustrate local fiber alignment; global structure must be inferred from architecture maps. (A) At 0 mmHg, the native vessel generally had a narrow, symmetric distribution, showing a high degree of alignment, while decellularized vessels typically had a wider, multi-peaked distribution, demonstrating less overall alignment and multi-directional orientation of fibers. (B) At 80 mmHg, native vessels had a slightly wider distribution, while the distribution for decellularized arteries became narrow and symmetric, showing higher local fiber alignment.

Table 1

Mechanical properties of native and decellularized arteries[a]

	Extensibility (%)	Tensile modulus (MPa)	Hysteresis (%)	Stress relaxation (%)
Native	79.18±5.70	2.29±0.24	31.55±12.60	45.96±9.31
Decellularized[a]	8.25±0.95*	3.48±0.72*	40.49±3.94	52.91±6.35

[a] Data show mean±standard deviation.

* Significantly different from native for $P<0.05$.